Investigations of the law-of-the-wall over sparse roughness elements

James King,[1] William G. Nickling,[2] and John A. Gillies[3]

Received 27 March 2007; revised 7 September 2007; accepted 9 November 2007; published 8 March 2008.

[1] This paper examines the application of the law-of-the-wall or gradient method for calculating the shear velocity, roughness length, and displacement height over three increasing roughness densities replicated with three different sized cubes within a recirculating wind tunnel. We compare these aerodynamic parameter estimates with estimates of the same parameters derived from other established methods: Reynolds stress analysis and the outer-layer velocity-defect law. By using more than one roughness height for the same roughness density (λ), dependencies of these parameters on roughness element height were also evaluated. Using the vertical wind speed logarithmic profile layer (determined graphically), resulted in shear velocity estimates that are greater by more than a factor of two than those determined using hot-film anemometry. The law-of-the-wall method provided a good estimate of the roughness length when applied to only that portion of the wind speed profile identified by Reynolds stress measurements to be within the constant stress layer; however, the shear velocity was overestimated by an average of 43% compared with that measured directly by hot-film anemometry. The best prediction of both of the roughness length and shear velocity, compared to estimates using Reynolds stress analysis, was obtained using the outer-layer velocity-defect law. We advocate that the velocity-defect law method be used in wind tunnel testing for calculating the shear velocity and roughness length from velocity profiles over sparsely spaced roughness elements, or when flow is highly heterogeneous, instead of the law-of-the-wall.

Citation: King, J., W. G. Nickling, and J. A. Gillies (2008), Investigations of the law-of-the-wall over sparse roughness elements, *J. Geophys. Res.*, *113*, F02S07, doi:10.1029/2007JF000804.

1. Introduction

[2] The application of the law-of-the-wall (logarithmic profile gradient method) to determine the aerodynamic properties of surfaces (e.g., shear velocity, u_*; aerodynamic roughness length, z_o; displacement height, d) in aeolian research has become increasingly contested because of the difficulty in clearly identifying and measuring within the region that the law-of-the-wall is valid (i.e., the inertial sublayer, *ISL*). Whether measuring a shear stress or velocity profile above sparsely distributed roughness elements or within saltating sediment, the location and depth of the *ISL* is not consistent. We carried out a wind tunnel study to examine the application of the gradient method for wind flow over sparsely distributed roughness elements and then compared and contrasted the aerodynamic parameter estimates obtained from applying the law-of-the-wall with those determined using two other methods: Reynolds stress analysis, and the outer-layer velocity-defect law approach. Reynolds stress analysis is a common method used in wind tunnel studies to determine surface shear stress [e.g., *Kaimal and Finnigan*, 1994; *Raupach et al.*, 1991], but the velocity defect approach is less well known [*Raupach et al.*, 2006].

[3] It is important that researchers be aware of the limitations of their measurement approaches. Therefore, the purpose of this paper is to illustrate the uncertainties associated with applying the law-of-the-wall in wind tunnel and field studies, a common measurement method in aeolian research, to characterize the boundary layer flow. This was achieved by systematically increasing the surface roughness in the wind tunnel over a range of different sized roughness elements to determine the effects of the different approaches on the critical parameter estimates as the number of roughness elements per unit area decreases.

2. Background

[4] The wind provides an applied tangential force (or shearing stress) to the surface. The flow of air over a surface with nonerodible roughness elements develops a continuum of layers that are characterized by the properties of the elements, as well as any upwind roughness. The inner layer contains the *ISL* and roughness sublayer [*Raupach et al.*, 1991]. The *ISL* is important to characterize because the Reynolds shear stress (τ_z) variation within this region is at a minimum [*Tennekes and Lumley*, 1972]. Within the surface

[1]Division of Atmospheric Sciences, Desert Research Institute, Las Vegas, Nevada, USA.
[2]Wind Erosion Laboratory, Department of Geography, University of Guelph, Guelph, Ontario, Canada.
[3]Particle Emissions Measurement Laboratory, Division of Atmospheric Sciences, Desert Research Institute, Reno, Nevada, USA.

0148-0227/08/2007JF000804

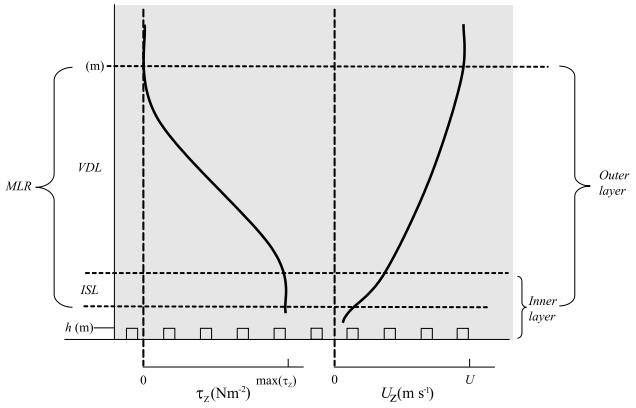

Figure 1. Schematic of a developed boundary layer (δ) over roughness elements of height, h (m). Plotted are interpretations of the Reynolds stress (τ_z) profile and velocity (U_z) profile. Also labeled are the zones identified within the text of the inertial sublayer (*ISL*), maximum logarithmic layer (*MLR*), and outer-layer velocity-defect law (*VDL*).

roughness elements turbulent mixing creates a flux of momentum towards the surface, which can be measured through the covariance between the instantaneous fluctuations of the vertical and horizontal velocity components within the *ISL* and is equated to the surface shear stress. A time-averaged vertical gradient of horizontal velocity within the *ISL* can also be related to the surface shear stress with a height-dependent eddy diffusivity [*Raupach et al.*, 1991; *Tennekes and Lumley*, 1972]. The estimation of the shear stress by measuring velocity profiles (gradient method) has been widely adopted among aeolian geomorphologists because of the robust nature of cup anemometers for field experiments and pitot tubes used in wind tunnels. However, the velocity profile measurement approach has limitations due to the vagueness of which portion of the profile is considered log-normal, the errors associated with the number and heights of the instruments that measure the profile [*Wilkinson*, 1984], and the variability in the surface parameters if the surface roughness is not homogenously distributed [*Gillette and Pitchford*, 2004; *King et al.*, 2006; *Raupach et al.*, 2006].

[5] The velocity profile above a roughened surface develops into an inner and outer layer. The velocity field within the inner layer is a function of the height, spacing, and shape of the roughness and the velocity field within the outer layer is not a function of any surface length scales (Figure 1). The *ISL* is the overlap region where the inner and outer layer are both valid and exhibits no more than 10% vertical variation in Reynolds shear stress (τ_z) from the maximum value [*Stull*, 1988]. The vertical profile of horizontal velocity in the *ISL* can be described by the inner layer application of the law-of-the-wall:

$$\frac{U_z}{u_*} = \frac{1}{\kappa} \ln\left(\frac{Z}{z_o}\right) \tag{1}$$

where κ is Von Kármán's constant (0.4), U_z (m s^{-1}) is the horizontal time-averaged velocity at a height z (m), z_o (m) is the aerodynamic roughness length and $Z = z - d$, with d (m) defined as the zero-plane displacement height [*Jackson*, 1981]. The shear velocity (u_*) characterizes the surface shear stress (τ_o) and is defined as $u_* = (\tau_o/\rho)^{0.5}$, where ρ is the fluid density.

[6] The vertical velocity profile is obtained by detailed measurements at incremental heights from typically twice the height of the roughness elements to 10 times the height of the roughness (h) [*Raupach et al.*, 1991]. The logistical constraints of capturing this layer in field measurements are imposed by the number and type of instruments available for use, data recording resources, and the height of the anemometry towers (typically 10–15 m). These limitations are minimized within laboratory wind tunnels by scaling the experiment to produce a boundary layer that develops beyond the surface layer. However, common to both field and wind tunnel studies is the varying depth of this layer when measured over roughness elements that are sparsely distributed, complicating its identification when not coupled with direct shear stress profile measurements.

[7] Theoretically, z_o and d are characteristic properties of a surface for fully turbulent flow and vary as a function of the roughness properties [*Kaimal and Finnigan*, 1994]. It has been suggested for natural vegetation that the use of one meteorological tower with cup anemometers to measure the vertical profile of time-averaged velocity can result in a variety of z_o and d values that are dependent on the wind direction [*Gillette and Pitchford*, 2004; *King et al.*, 2006] because of the variable alignment of natural roughness. In laboratory investigations however, this variability can be constrained by uniform roughness distribution, the ability to spatially average profile measurements, and/or unidirectional flow.

[8] The value of d can be found by a least squares fit of u_z against equation (1) to the *ISL* portion of the profile by calculating the centroid of the drag profile within the roughness [*Thom*, 1971] or through an a priori empirical relationship such as the one from *Raupach* [1994] or *Macdonald et al.* [1998]. The calculations of d can also be based on u_* as determined from the measured velocity or shear stress profile ($\tau_o = -\rho\overline{u_z' w_z'}$). The determination of z_o is calculated with equation (1) with u_* as the slope, requiring some portion of the fluid flow to be described by the *ISL*.

[9] The outer-layer velocity-defect $U_\delta - U_z$ (δ is boundary layer depth) depends on u_*, z, d and outer-layer length scales. In a canonical boundary layer, defined as one with zero pressure gradient, having a uniform surface roughness element distribution, and no leading roughness features, the outer-layer length scales can be considered constant as measured by *Clauser* [1956]. *Raupach et al.* [2006] simplified the measurements of *Clauser* [1956] into the empirical model:

$$\frac{U_\delta - U_z}{u_*} = B + \frac{\eta}{\kappa} - \frac{B}{1 + (\eta/\eta_0)^n} \tag{2}$$

With $\eta = -\ln(Z/\delta)$ and $\eta \geq 0$. *Raupach et al.* [2006] suggest, on the basis of a review by *Hinze* [1975], values of $B = 2.5$, $\eta_0 = 1$, and $n = 3$. For the calculation of z_o from measurements within the outer-layer, the inner- and outer-

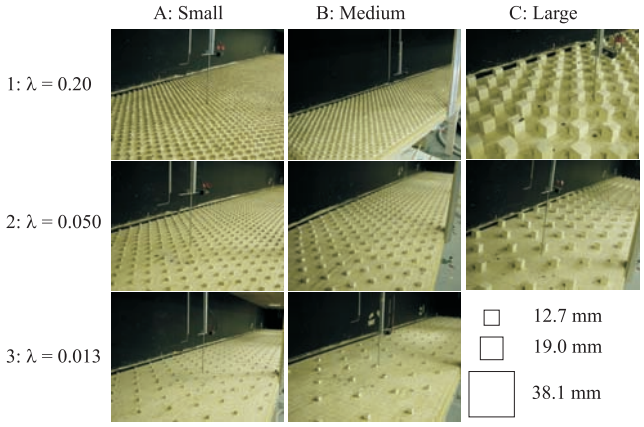

Figure 2. Photographs of the element configurations for all runs.

layer logarithmic portions from the inertial layer can be combined for the solution:

$$\frac{z_o}{h} = \frac{\delta}{h} \exp\left[\kappa\left(B - \frac{U_\delta}{u_*}\right)\right] \tag{3}$$

[10] *Raupach et al.* [2006] derived these functions because of the heterogeneity within the *ISL*, which they observed in a wind tunnel study over sparsely spaced roughness elements ($h/\delta > 0.02$), and in particular when roughness elements are clustered or randomly organized. Within the sparse roughness configuration they were examining, *Raupach et al.* [2006] argued that no *ISL* could be identified from Reynolds stress or velocity profile measurements over the clustered or randomly spaced roughness elements. The roughness element distributions utilized in their experiments were too complex to facilitate any direct comparisons for the finite values of u_*, z_o/h and d from the aforementioned methods. In our experiment we used organized staggered arrays of roughness elements with significant fetch, which allowed us to evaluate differences in u_*, z_o/h and d calculated by the three different methods to highlight their varying accuracies.

[11] Roughness elements can be composed of different types of vegetation, large rocks or boulders, or sand fences, and their size, shape, and density depend on the specific environment. However, as the wind is displaced by a roughness element it is locally accelerated, increasing the heterogeneity of the near-surface flow that is likely to aid in locally eroding the soil surface [*Glendening*, 1977]. Introducing nonerodible roughness elements onto a surface leads to an overall increase in shear stress above the roughness elements, but depending on the density of the roughness elements, they can also cause localized increases in shear stress around the elements or an overall decrease in the shear stress [*Gillies et al.*, 2007]. The roughness elements also cover a portion of the erodible surface and can act to reduce the amount of sediment in transport by operating as a physical barrier [*Gillies et al.*, 2006].

[12] Surface roughness elements can be represented in an ensemble sense, based on the geometry, distribution, and/or aerodynamic properties of a given array. The most common surface roughness descriptor is roughness density, λ defined as:

$$\lambda = \frac{nbh}{S} \tag{4}$$

with b and h being the average width (m) and height (m) of the individual roughness and n being the number of roughness elements in a given surface area, S (m^2). Even though the requirements for measuring λ are well defined in the literature for solid geometrically simple roughness, there are complications when calculating for roughness that consists of varying heights, widths, and lengths or in the case of vegetation different porosities. Surface roughness when defined by its physical properties (e.g., λ) allows for a simple approximation of its influence on the boundary layer flow when an area can only be assessed remotely. The use of λ is frequent because of its strong correlation with the aerodynamic effects of the roughness as empirically correlated by z_o/h [*Lettau*, 1969; *Raupach*, 1994].

3. Methods

[13] The experiments for the present study were conducted in the University of Guelph, Wind Erosion Laboratory, recirculating wind tunnel [*Gillies et al.*, 2002]. This wind tunnel is powered by a 1.0 m axial vane fan powered by a digitally controlled, variable AC motor. The tunnel's corners are redirected through turning vanes and the flow is straightened through a honeycomb section followed by a 2.8:1 contraction section before entering the working section. The working section is constructed of a varnished plywood floor, measuring 8.0 m long, 0.76 m high, and 0.92 m wide. A moveable pitot-static tube attached to a stepper motor and connected to a differential pressure transducer (ThermBrandt Ltd, (12 mm water head) Transducer; Model DPT 32S12-0.5; precision ±0.25% full scale) with Tygon tubing is used to monitor the freestream velocity and to calibrate other instrumentation. In addition, pressure taps at the front and rear of the working section, 100 mm below the ceiling and connected to a manometer with tubing was used to monitor pressure changes down the length of the working section.

[14] For the surface roughness, three different sized cubes were used and arranged to acquire three different roughness densities (Figure 2). To examine the appropriateness of the application of λ as a descriptor of the roughness, we chose three sizes that allowed for a large enough change in height without exceeding the limits of the wind tunnel dimensions. The spacing of the elements produced λ values of 0.20, 0.050, and 0.013 for all but the largest cubes. The interelement spacing is described in Table 1. This facilitated measurements for three replications of the same λ value with three different element sizes of the exact same shape (except for the lowest λ which only had two replicates). The roughness was placed onto plywood sheets at the most dense spacing for each size and filled the entire working section of the wind tunnel floor. The next λ value was established by systematically removing every other roughness element in a row and every other element row (Figure 2). This process was repeated for the small and medium cubes to obtain the least dense spacing.

Table 1. Geometric Properties of the Wind Tunnel Configurations

Surface	A1	A2	A3	B1	B2	B3	C1	C2
Cube length (mm)	12.70	12.70	12.70	19.05	19.05	19.05	38.10	38.10
Roughness concentration (λ)	0.20	0.050	0.013	0.20	0.050	0.013	0.20	0.050
Downwind spacing (mm)	20.0	40.0	80.0	30.0	60.0	120.0	65.0	130.0
Crosswind spacing (mm)	40.0	80.0	160.0	60.0	120.0	240.0	130.0	260.0

[15] Hot-film anemometry (*HFA*) was used to measure the streamwise and vertical velocities at a series of heights (z) above the roughness. Measurements were made using a platinum cross-film anemometer (Model 1241-20, TSI, Inc.) having film lengths of 1.02 mm and diameter of 50.8 μm, with an included angle of 90°. The anemometry sampling was controlled by ThermalPro (TSI Inc.) software and recorded through a 16 bit PowerDAQ A/D board with a PC. The probes were calibrated with a pitot-static tube at the beginning of each set of runs at a height of 450 mm through 15 wind speeds and nine angles (10° increments). The probe was located in the working section at a length of 6.8 m from the leading edge of the roughness elements and mounted on a vertical stepping motor. The recorded signal was corrected for any misalignment into the flow by computationally aligning the top measurement (within freestream) to equate the average vertical velocity to zero. This instrument was sampled and recorded at 600 Hz with a low pass filter at 100 Hz and a sampling time of 20 s. Additionally, the horizontal velocity was correlated with the pitot-static tube measurement at the beginning of each run to minimize any horizontal misalignments. Only the corrected data are used in this paper.

4. Results

[16] The calculation of u_* by equation (1) and equation (2) requires a determination of the *ISL* region and δ, respectively. However, in most aeolian field measurements the direct determination of the constant shear stress layer is physically unattainable since the anemometry that can measure in more than one dimension at a high frequency (hot-wire or sonic anemometry) cannot withstand sediment transport activity. In field conditions, equation (1) has typically been applied by choosing a section of the measured wind velocity profile that appears to be log-linear and will also be below the top of the boundary layer (when detected).

[17] It is of importance to apply the same method to the measurements made in this study and compare any differences in the computed u_* and z_o values to those estimated using more robust methods. This method includes the maximum number of measurement points within the vertical wind speed profile (while maintaining the maximum regression coefficient) to calculate these parameters and is denoted as the maximum logarithmic region (*MLR*) method. We identify parameter estimates derived from this method with the subscript *MLR*. We also directly measured the shear stress in the *ISL* region using the *HFA* by applying Reynolds stress techniques. Parameter estimates derived from Reynolds stress measurements are subscripted *uw*. Once the *ISL* was identified using the *HFA* (and is defined as the region where Reynolds stress values vary <10% from the maximum [*Stull*, 1988]), a second estimation of u_* and z_o using the gradient method but using only horizontal wind speeds measured in the *ISL* was calculated. This is referred to as the *ISL* method and parameter estimates derived from this method are denoted with the subscript *ISL*. The calculation of u_*, z_o, and d using equation (1) for both the *MLR* and *ISL* gradient methods was performed using a stationary iterative method for convergence on a resulting d that best explained the measured logarithmic height and wind speed relationship. When a value of d was solved that was less than zero, it was set to zero due to the physical impossibility of $d < 0$ in a laboratory configuration.

[18] A third method, the outer-layer velocity-defect law (*VDL*, equation (2)), was also used to estimate the aerodynamic parameters for each roughness condition. The *VDL* method was used to calculate u_* from the horizontal velocity measurements and the boundary layer height. This method requires a canonical boundary layer, which is satisfied by our experimental setup by having a horizontally uniform surface, a boundary layer developed without any tripping devices, and a near-zero pressure gradient (as discussed in the following section). The results obtained with this method are compared with those estimated using both gradient method approaches (*MLR* and *ISL*) and from the Reynolds stress approach. The outer-layer velocity-defect law was calculated by fitting the velocity profiles to the measurements of *Clauser* [1956] as modeled by equation (2) and using u_* and δ as parameters to obtain the best-fit solution (Figure 3). As suggested by *Raupach et al.* [2006], the zero-plane displacement height was calculated from the following d/h relationship a priori with the recommended parameter values [*Raupach*, 1994] to obtain:

$$\frac{d}{h} = 1 - \frac{1 - \exp\left(-\sqrt{15\lambda}\right)}{\sqrt{15\lambda}} \tag{5}$$

4.1. Hot-Film Anemometry (HFA)

[19] The *HFA* data were used to identify the *ISL* as indicated by the zone of constant stress and to determine an average u_* using Reynold's stress analysis (i.e., $u_{*_{uw}}$). The average U_z values obtained with the *HFA* were also used for calculating u_{*MLR} and u_{*ISL} using equation (1).

[20] In Figures 4, 5, and 6, τ_z is plotted for each λ to show the differences in τ_z over the range of densities. There are two notable trends; the first is in all cases there is an increase in τ_z as $z \rightarrow 0$; the second is the increase in the maximum τ_z with increasing λ for the same freestream wind speed. These profiles are characteristic for flow over a rough boundary but because of wind tunnel dimension constraints the depth of the constant stress layer is limited. There is a decrease in τ_z toward the surface within the *ISL* region that could be due to pressure increases or the

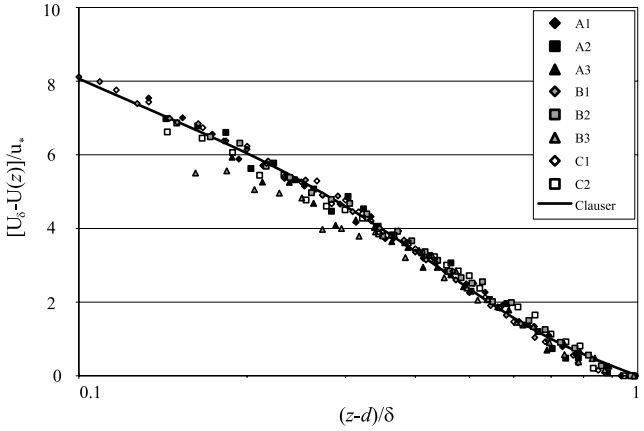

Figure 3. Mean velocity profiles plotted as outer-layer dimensionless form. The line is from the canonical profile model of *Clauser* [1956].

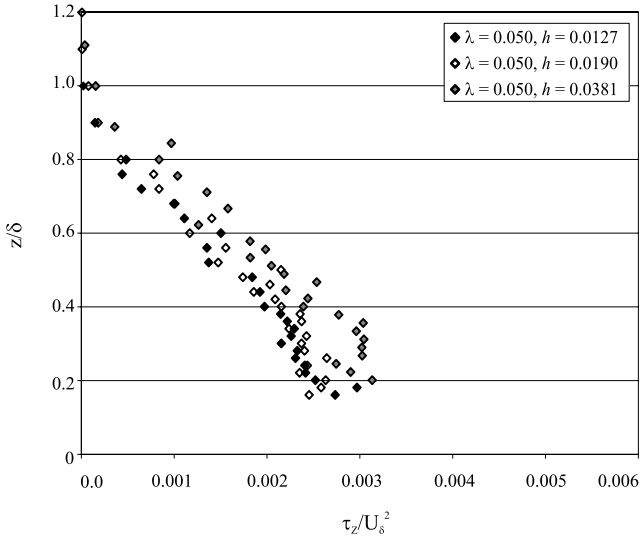

Figure 5. Height normalized by boundary layer depth (z/δ) plotted with normalized Reynolds shear stress (τ_z/U$_\delta^2$) of all element sizes for λ = 0.050.

growing boundary layer down the length of the wind tunnel, although the pressure differences were adjusted beyond the working section with a series of screens to maintain a minimum pressure increase (Δ static pressure/dynamic pressure <5%). The pressure gradient must be negligible to conform to the canonical boundary layer assumptions and would introduce errors into applying the velocity defect law to the experimental results. It was noted by *Raupach et al.* [2006] that the ratio of the momentum loss due to the growing boundary layer to the momentum provided by the pressure gradient, was approximately 5:1 for their experiments suggesting that the flow conforms to the canonical boundary layer requirements. Within this experiment multiple streamwise profile measurements were not made; however, we assume that the results from *Raupach et al.* [2006] would be applicable because of the less complex arrangement of the roughness in this experiment. Therefore, the substantial decrease observed in the shear stress as the surface is approached is likely from increasing errors in the *HFA* signal as the turbulence intensity increases towards the surface. Regardless, this decrease in τ_z toward the surface signifies that the measurements at that point are below the *ISL* region. Therefore, the profiles of τ_z obtained incorporate the maximum τ_z value over each surface (within the *ISL*), providing a direct comparison with the estimates of u_{*MLR}, u_{*ISL}, and u_{*VDL}.

[21] The difference in τ_z with dimensionless height for the same λ (but different sized cubes) is shown in Figures 4, 5, and 6. For λ = 0.20, this difference is clearer (Figure 4) than for λ = 0.05 and λ = 0.0126 (Figures 5 and 6). Although the differences exist, the average shear stress value for the *ISL* is primarily dependent on the density of the roughness and only secondly on the size of the roughness. Whether this difference is also evident in the calcu-

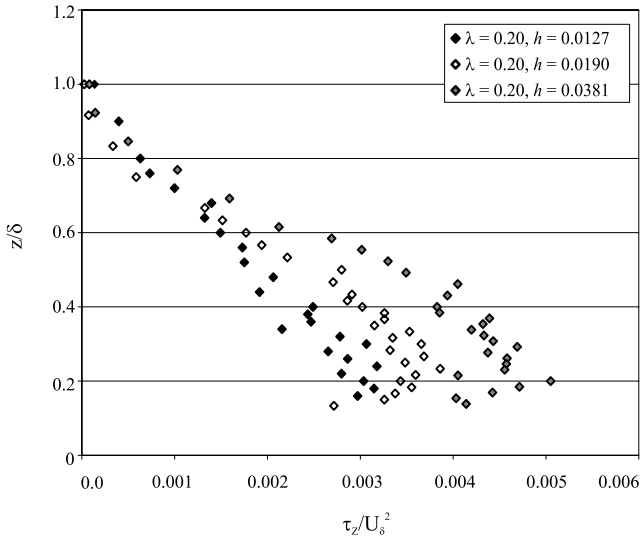

Figure 4. Height normalized by boundary layer depth (z/δ) plotted with normalized Reynolds shear stress (τ_z/U$_\delta^2$) of all element sizes for λ = 0.20.

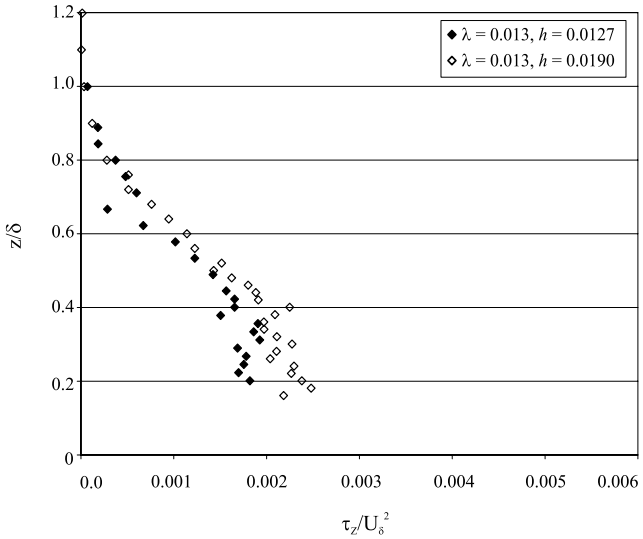

Figure 6. Height normalized by boundary layer depth (z/δ) plotted with normalized Reynolds shear stress (τ_z/U$_\delta^2$) of all element sizes for λ = 0.013.

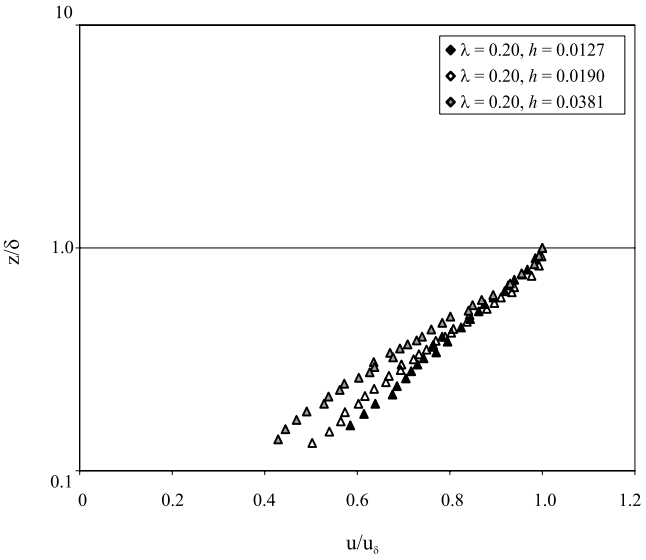

Figure 7. Height normalized by boundary layer depth (z/δ) plotted with velocity normalized with velocity at δ for λ = 0.20 for all cube sizes.

lated u_* values from the gradient and *VDL* methods will be discussed later.

4.2. Law-of-the-Wall Determination of u_*, z_o, and d

[22] Using the velocity profiles for $\lambda = 0.20$ as shown in Figure 7, it appears plausible that a continual log-linear trend exists from the bottom-most measured points to slightly below the freestream portion (U_δ) of the flow. Although this is unrealistic based on the τ_z profiles and violates the principles for the log law to hold, it is evident that the depth of the inner layer is difficult to predict accurately without direct stress measurements. However, by plotting the profile as Z/z_o against U/u_* (see Figures 8a–8h) a small portion of the lower vertical wind speed profile within the constant stress layer as determined by the *HFA* appears log-linear in form. As well, the overall measured profile displays a pronounced kink at the top of the outer layer that increases with cube size. The least dense arrays also have significant deviation from the law-of-the-wall profile in the upper portion of the velocity profiles (Figures 8c and 8f).

[23] Table 2 shows the calculated u_*, d, and z_o values from the *ISL* and *MLR* methods for all λ values. This was calculated in two different ways. In the first calculation we apply the gradient method (labeled *ISL*) for wind speeds of heights known to be within the *ISL* region (through identification by the *HFA*) are used, and the logarithmic profile is solved using equation (1) by varying d to maximize the regression coefficient between $\log(Z)$ and U_z. For the other application of the gradient method (labeled *MLR*) we calculate u_*, d, and z_o from equation (1) as is common in most aeolian field studies (i.e., the log-linear layer is determined from the vertical velocity profile without directly identifying the *ISL* but from maximizing the regression coefficient of wind speed against logarithmic height). Identical to the method for calculating the *ISL* values, the iterative best-fit stationary method for solving equation (1) was used.

[24] Comparing first the values of u_* calculated, $u_{*MLR} > u_{*ISL} > u_{*uw}$ (Table 2). This difference becomes minimized when $d > 0$ and as a result, z_{oMLR} and u_{*MLR} decrease; however, none of the methods resulted in a $d > 0$ for the *MLR* method. This pattern may well be an artefact of the shape of the velocity profile because within the *ISL* it is more likely that $d > 0$ (when iteratively solved) in comparison to $d = 0$ when solved using the *MLR*-designated approach. With $d > 0$, u_{*ISL} is consistently less than u_{*MLR}, suggesting that the incorrect application of the ''law of the wall'' when the *ISL* region is not explicitly known could lead to overestimating the protection that the roughness provides for the surface from the shear stress partitioning relationship developed by *Raupach et al.* [1993].

[25] The u_{*uw} values represent the magnitude of the constant stress layer and therefore are regarded as the most accurate estimate of the total stress created by the rough surfaces. The values for u_{*uw} with increasing height of the roughness (but same freestream wind speed) are displayed for the all λ values in Figure 9. These data exhibit a positive slope (Figure 9), suggesting that u_{*uw} may have an additional dependency on the height of the roughness as well as the spatial arrangement of that roughness. However, this pattern is only clear for $\lambda = 0.20$, while further supporting data are required to suggest a universal trend with λ. The larger u_{*uw} for the larger roughness can also be visualized by plotting it against λ as grouped by roughness size (Figure 10). This figure shows two characteristic patterns: the first is that the difference in the u_{*uw} measured for the same λ for the different sized roughness increases with increasing λ; and second, the larger roughness always has a higher u_{*uw} for the same λ. However, this trend is also not completely clear because for $\lambda = 0.05$ the h = 19.05 mm (medium) roughness has a lower u_{*uw} than for the h = 12.70 mm (small) roughness. This discrepancy could be resolved with a larger range of element heights in addition to different types of roughness elements.

[26] The u_{*ISL} values are consistently less than those calculated using a greater portion of the velocity profile (*MLR*) (Table 2). The main differences in these two applications of equation (1) are that for the majority of the cases, using the entire velocity profile up to U_δ results in $d = 0$ (or $d < 0$, which was then set to a value of zero). Having a displacement height greater than zero in equation (1) reduces u_* and z_o, resulting in u_{*ISL} being around approximately half the u_{*MLR} value. Additionally, z_o values calculated using data just from the identified *ISL* region are over an order of magnitude lower than their values when $d = 0$ as calculated with the *MLR* approach. When applying equation (1) under the *MLR* assumption, higher values of both z_o and u_* are estimated, which can give a false indication of the true magnitude of the surface roughness.

4.3. Outer-Layer Velocity-Deficit Law (VDL)

[27] Shear velocities calculated using the outer-layer velocity defect law are subscripted *VDL* and are tabulated with the u_* values estimated by the other methods in Table 2. For most λ configurations, the values of u_{*VDL} are greater than u_{*uw}; however, this method yields values of u_* never in excess of the values obtained from either of the law-of-the-wall methods (i.e., *MLR* and *ISL*). The u_{*ISL} values are at a minimum 25% greater than the u_{*uw} values,

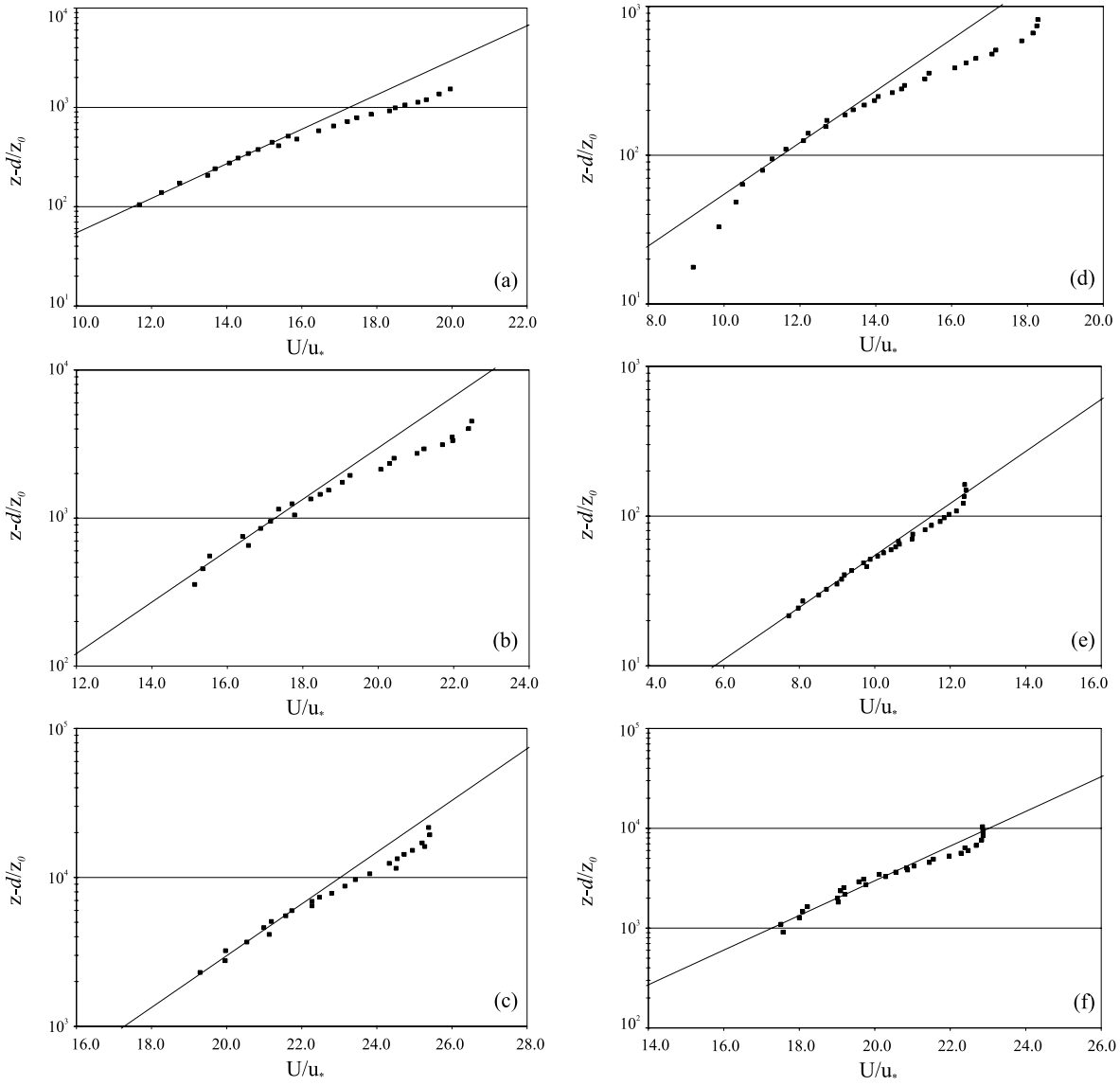

Figure 8. Logarithmic profile normalized height ($z\text{-}d/z_o$) plotted with dimensionless velocity (U/u_*) for the small cube at (a) $\lambda = 0.01$, (b) $\lambda = 0.050$, and (c) $\lambda = 0.013$, for the medium cube at (d) $\lambda = 0.01$, (e) $\lambda = 0.050$, and (f) $\lambda = 0.013$, and for the large cube at (g) $\lambda = 0.20$ and (h) $\lambda = 0.050$. Solid line is the law-of-the-wall.

while u_{*VDL} values are never ±10% different than u_{*uw}. Fitting the profiles to the *Clauser* [1956] canonical model provided correlation coefficients >0.990 for all surfaces (Table 2) indicating the good agreement of this method to profiles measured at one location above a sparse regular array of roughness elements.

5. Discussion

[28] Comparing the values of the aerodynamic characterization parameter estimates derived using the methods described above offers insight into how choosing different methodological and associated analytical approaches to characterize boundary-layer flow over sparse roughness elements can affect the interpretation of the relative importance of the roughness to modify the total shearing stress in the above element flow. The subsequent estimates of the shear stress that can reach the surface among the roughness elements from these different methods are also important when considering wind erosion modelling.

[29] The results from the *HFA* measurements to estimate u_* indicated that there was a secondary dependence on the height of the roughness elements for the same λ, suggesting λ is not a true independent variable for evaluating surface roughness effects on z_o/h. However, the trend shown in u_{*uw} (Figure 9) and from u_* from the other methods (Table 2) is not conclusive based on the limited data set collected in this study. If this experiment was extended to a range of element heights that vary over more than one order of magnitude (not physically possible in the wind tunnel used in this study), the differences could be significant. This would alter the well-established empirical hypothesis that λ is an

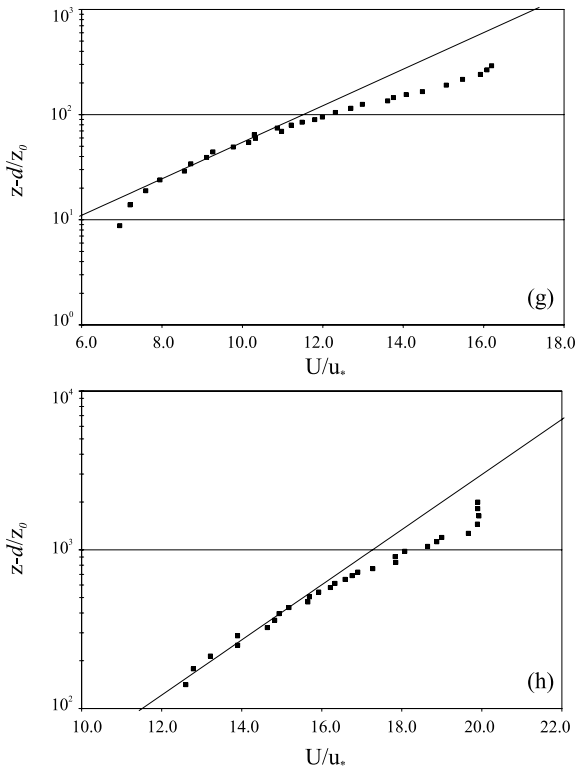

Figure 8. (continued)

independent variable for surface roughness and could explain a portion of the scatter amongst parameters using λ as a dimensionless roughness scale. Previous research has investigated the effects of aspect ratios [e.g., *Marshall*, 1971; *Musick et al.*, 1996; *Crawley and Nickling*, 2003]; however, most aeolian roughness elements do not deviate far from an aspect ratio of unity. Therefore, independent of λ, a large difference in the height of roughness elements could alter the partition of stress between the roughness and the surface.

[30] The dimensionless aerodynamic roughness of z_o/h within sparse roughness has been commonly described as a function of λ. In Figure 11 the empirically based models of *Lettau* [1969] and *Raupach* [1994] are plotted as two examples of this inferred relationship. The performance of both field data and laboratory data from previous studies has been shown to fall predictably well around these two models despite the log-log scale [*King et al.*, 2005]. The values of z_o/h for each λ in this experiment using all three methods to define z_o are plotted in Figure 11. A considerable spread (over an order of magnitude) in the z_o/h values for the same λ exists. The two solutions from the law-of-the-wall method (both *ISL* and *MLR*) on average overestimate the model values, while the *VDL* z_o/h method underestimates the modeled values. The best agreement with the *Lettau* [1969] empirical model is with the *VDL* z_o/h values, while the z_o/h values calculated using the law-of-the-wall for wind speeds constrained within the *ISL* region are in the best agreement with the *Raupach* [1994] model. The variation in z_o/h for the law-of-the-wall calculations using either the *ISL* or *MLR* approaches is relatively large (note the log-log scale) due to the large variations of d that are estimated, despite their lower coefficients of variation of z_o/h for the same λ than the other methods. The discrepancy shown in Figure 11 between the z_o/h estimates and the two models can be partly attributed to the d values that are resolved from the different methods as well as the measurement errors previously mentioned [*Raupach et al.*, 2006; *Wilkinson*, 1984], which are associated with measuring velocity profiles over sparsely spaced roughness elements. These trends suggest that the velocity profiles over the sparse roughness can be used with some confidence when measured within the *ISL* to calculate z_o and u_*, but not d when only measured at one location.

[31] The spread in z_o/h for the same λ values is not surprising, in that each λ value is represented by different sized cubes in contrast to repeated trials of the same configuration. From the expression suggested by *Raupach et al.* [2006] (Table 2 *VDL* values of d), the values of d iteratively solved for using just the wind speed data in the *ISL* were very similar to the d predicted for the largest roughness size except when (half of the surfaces) a value of $d = 0$ was assigned. However, a value of $d = 0$ was assigned (because of the nonsensical d values that resulted) for all roughness arrangements when using the *MLR* approach, even though a d value ranging from 2 mm and 20 mm was predicted by *Raupach et al.* [2006] for $\lambda = 0.013$ of h = 12.07 mm and $\lambda = 0.20$ for h = 38.10 mm, respectively, further emphasizing the violation of the log law. For the smallest λ the suggested d values from *Raupach* [1994] are all below 4 mm.

[32] The values of u_* derived from the different methods also vary considerably. Taking the value of $u_{*_{uw}}$ calculated from the constant stress profile measured by the *HFA* as the best approximation of the overall shear velocity, the other values range from a slight underestimation to a factor of two overestimation. The largest discrepancy is for the $u_{*_{MLR}}$ value, where the smallest difference is still 30% greater than the $u_{*_{uw}}$ value with an average overestimate in u_* of ~70%. The value of u_* calculated from just the *ISL* region using the law-of-the-wall, overestimates on average 43% compared with $u_{*_{uw}}$, with an overestimate of only 23% for the smallest λ configuration. The error associated with the calculation of these values (velocity gradient method) can be assessed by using the technique of *Wilkinson* [1984], which calculates the error of u_* and z_o based on the correlation coefficient from the gradient method in addition to the number and heights of the velocity points used within the method. This method shows the errors (at a 95% confidence limit) in u_* do not exceed 0.09 m s^{-1}, corresponding to a maximum of ±10% for that value (Table 2). The error resulting from the uncertainty in the calculations using the gradient method in part explains the overestimation arising from this method. However, the $u_{*_{MLR}}$ values are outside the 95% confidence level of agreement with $u_{*_{uw}}$ suggesting that the values are significantly different. For the smallest λ, $u_{*_{ISL}}$ is not significantly different at the 90% confidence level but is different at the 95% level, while for the other roughness densities $u_{*_{ISL}}$ is significantly different even at the 90% level. This is in contradiction with the initial premise that an increase in error would be associated with an increase in roughness interelement spacing (in this case a decreasing λ). This assumption holds for the calculation of z_o/h, but it seems in that for calculating $u*$, the slope of the velocity

Table 2a. Aerodynamic Properties of the Wind Tunnel Configurations As Calculated From Hot-Film Anemometer (*HFA*), Velocity-Defect Law (*VDL*), and Logarithmic Profile From the Inertial Sublayer Region (*ISL*) and the Maximum Logarithmic Layer (*MLR*)[a]

	Low	Top	z_o (m)	d (m)	R^2	u_* (m s^{-1})
			A1			
VDL			4.73E-04	0.0067	0.998	0.591
HFA	40	75				0.590
ISL	40	75	2.15E-03	0.0052	0.988	0.908
MLR	40	225	3.22E-03	0.0000	0.997	1.002
			A2			
VDL			1.31E-04	0.0042	0.996	0.543
HFA	50	85				0.566
ISL	50	85	6.71E-04	0.0015	0.875	0.765
MLR	50	225	1.64E-03	0.0000	0.989	0.943
			A3			
VDL			2.20E-05	0.0024	0.996	0.438
HFA	40	80				0.481
ISL	40	80	1.38E-04	0.0000	0.960	0.602
MLR	40	200	2.47E-04	0.0000	0.992	0.667
			B1			
VDL			1.20E-03	0.0100	0.999	0.695
HFA	55	100				0.672
ISL	55	100	6.10E-03	0.0000	0.992	1.172
MLR	55	250	7.58E-03	0.0000	0.997	1.282
			B2			
VDL			4.00E-04	0.0063	0.997	0.604
HFA	40	80				0.556
ISL	40	80	1.85E-03	0.0000	0.985	0.898
MLR	40	200	2.55E-03	0.0000	0.995	1.011
			B3			
VDL			4.37E-05	0.0036	0.989	0.459
HFA	45	75				0.526
ISL	45	75	2.54E-04	0.0000	0.929	0.649
MLR	45	200	3.28E-04	0.0000	0.978	0.676
			C1			
VDL			2.28E-03	0.0200	0.999	0.743
HFA	60	100				0.744
ISL	60	100	3.43E-03	0.0230	0.978	0.913
MLR	60	275	1.37E-02	0.0000	0.997	1.449
			C2			
VDL			4.43E-04	0.0126	0.995	0.593
HFA	45	80				0.590
ISL	45	80	1.99E-03	0.0045	0.968	0.890
MLR	45	200	3.15E-03	0.0000	0.993	0.999

[a]Aerodynamic properties are lower and top heights (mm) of the profiles, roughness length (z_o) (m), displacement height (d) (m), regression coefficient (R^2), and shear velocity (u_*) (m s^{-1}).

profile would have to be significantly steeper than suggested by the *HFA* method derived $u_{*_{uw}}$. With the roughness elements being sharp-edged cubes, an increase in momentum absorbed by the elements in the horizontal direction could have contributed to a large gradient in the average horizontal values that does not translate into high shear stress values.

[33] The other possibility is that $u_{*_{uw}}$ values are significantly lower than they should be, however the values obtained by the *VDL* approach suggest otherwise. The $u_{*_{VDL}}$ values are on average only 2% lower than $u_{*_{uw}}$, with no discernable trend based on element size or spacing. From the measurements collected over random and clustered element arrays by *Raupach et al.* [2006], they found that this method provided the only means to estimate a realistic value of u_*. In our cases, the elements are a simpler staggered array suggesting that the *VDL* method would be in better conservation of the canonical boundary layer and lead to a better estimation of u_*. The errors associated with the *VDL* are only slightly greater than those that result from applications of the law-of-the-wall; however, even with these included, the close agreement among the aerodynamic parameter values as calculated by the *VDL* method and the Reynolds stress analysis approach (*HFA*-method), shows the *VDL* approach is superior to the gradient method for this application.

6. Conclusions

[34] In measurements of wind over varying roughness densities we observed significantly different estimates of u_*, z_o, and d when comparing between three different estima-

Table 2b. The 95% Confidence Limit Error of z_o and u_* of the *ISL* and Number of *ISL* Samples (n_{ISL}) for All Roughness Element Configurations

	h/δ	z_{oISL} error	$u*_{ISL}$ error	n_{ISL}
A1	0.051	1.58E-04	0.024	8
A2	0.051	2.46E-04	0.090	8
A3	0.056	5.39E-05	0.063	9
B1	0.070	1.63E-04	0.014	10
B2	0.085	1.48E-04	0.026	9
B3	0.085	1.23E-04	0.090	7
C1	0.127	2.65E-04	0.028	9
C2	0.169	2.32E-04	0.038	8

tion methods. The first was the gradient method (i.e., the law-of-the-wall), the second method was the direct measurement of the constant stress layer (Reynolds stress approach) and the third was the outer-layer velocity-defect approach.

[35] In the first approach we chose to follow a method typically used in field studies, which is to fit the logarithmic regression to velocity profiles from the apparently log-linear portion of the velocity profile, which does not take into account any knowledge of where the constant stress layer is actually located. In a second application of the gradient method we first identified the *ISL* using the *HFA* and then used only wind speeds at heights known to be in the *ISL* to calculate u_*, z_o, and d. Comparing the shear velocities estimated by these two methods with those obtained from Reynolds stress analysis, the u_* values calculated by the law-of-the-wall within the *ISL* were almost 50% more than those derived from the Reynolds stress method, while u_* calculated from the entire log-linear portion of the profile below the boundary layer height are double the u_* from the Reynolds stress analysis. Despite these differences in u_*, the z_o/h values calculated by the law-of-the-wall method from both regions correspond quite well to modeled, field and laboratory z_o/h data.

[36] The best estimates of u_* and z_o were calculated from the outer-layer velocity-defect law model presented by *Raupach et al.* [2006]. Both u_* and z_o/h from the *VDL* method compared favorably with the Reynolds stress-derived estimates of u_* within 95% and 90% confidence levels, respectively. The procedure for calculating these parameters for this method was less subjective than the law-of-the-wall method and does not require measurements close to the roughness elements themselves. However, the use of this method in field experiments is not possible because the atmospheric boundary layer does not conform to the conditions of the canonical boundary layer (zero pressure gradient, nonturbulent free stream, and a self-grown boundary layer).

[37] In conclusion, although a logarithmic profile of horizontal velocity may be observed, the application of

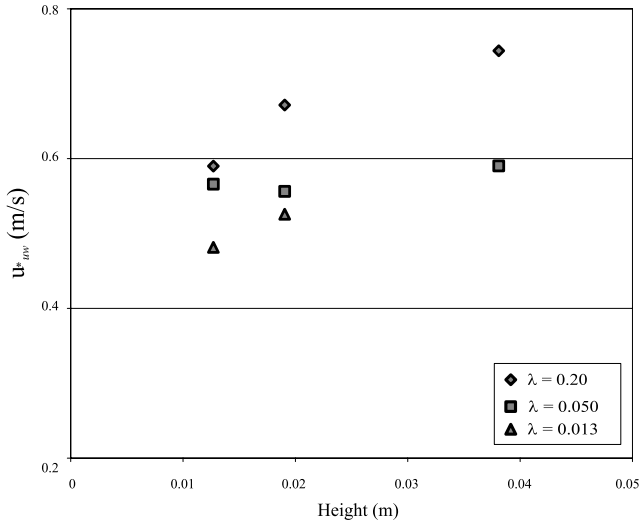

Figure 9. Shear velocity calculated from *HFA* within the *ISL* (u_{*uw}) plotted against the cube size and grouped by λ.

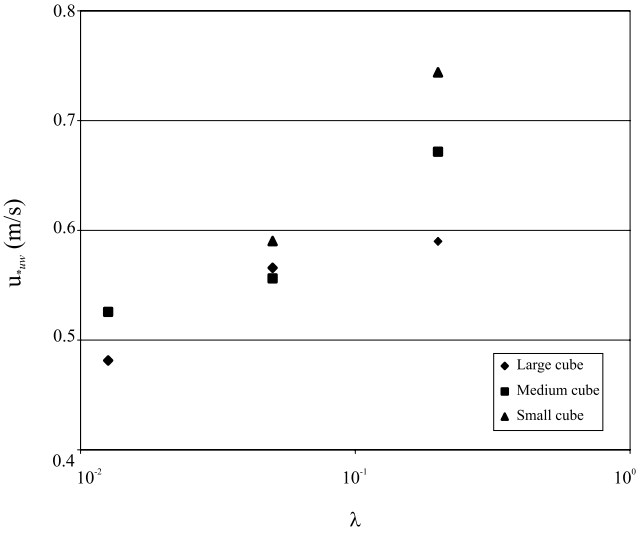

Figure 10. Shear velocity (u_{*uw}) calculated from HFA plotted against λ grouped by cube size.

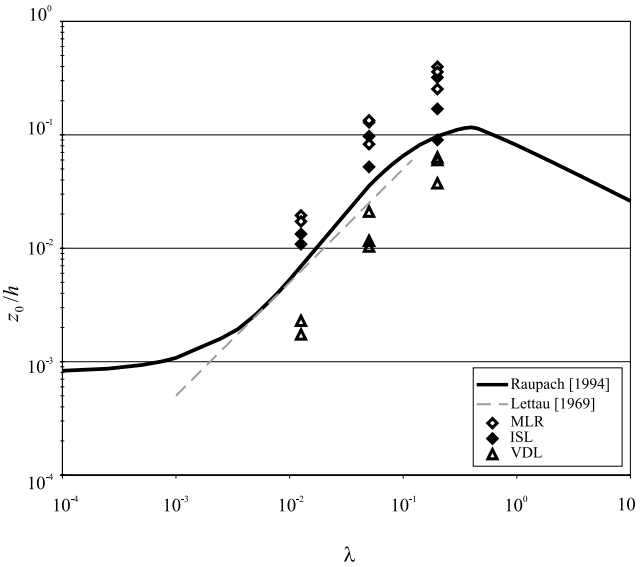

Figure 11. Roughness length normalized by element height (z_o/h) plotted against λ calculated from the velocity profile fitted to the inertial sublayer (u_{*ISL}) and the maximum logarithmic region (u_{*MLR}), and the calculated z_o/h from the velocity-defect law (VDL). Also plotted are the models of *Lettau* [1969] and *Raupach* [1994].

the law-of-the-wall likely produces erroneous shear stress estimates if the *ISL* is not correctly identified. This effect lessens with decreasing λ despite the heterogeneity of the surface at the lower λ. This reduces the complexity previously associated with calculating u_* and z_o amongst sparse ($\lambda < 0.1$) environments [*Gillette and Pitchford*, 2004; *King et al.*, 2006] but still requires field scale validation because of potential scaling effects. Undoubtedly, more replicate measurements of both laboratory and field data are required for low λ ranges with differently shaped roughness elements but this investigation hints at the large variations in boundary layer parameters that can be calculated from using an incorrect application of a method. This investigation also recommends the use of the outer-layer velocity-defect law when measuring velocity profiles over sparsely spaced roughness elements in wind tunnel experiments, as this method contains a smaller fraction of the uncertainties associated with the application of the law-of-the-wall.

[38] **Acknowledgments.** J. King and W. G. Nickling gratefully acknowledge the financial support of the Natural Sciences and Engineering Research Council of Canada (grant 7427-02). J. A. Gillies and W. G. Nickling gratefully acknowledge the support, of the NASA, Mars Fundamental Research Program (grant NAG5-12759). We would also like to thank Mario Finoro and Sandy McLaren, Geography Department, University of Guelph, for their technical support during the wind tunnel experiments.

References

Clauser, F. H. (1956), The turbulent boundary layer, *Adv. Appl. Mech.*, *4*, 1–51.

Crawley, D. M., and W. G. Nickling (2003), Drag partition for regularly-arrayed rough surfaces, *Boundary Layer Meteorol.*, *107*, 445–468.

Gillette, D. A., and A. M. Pitchford (2004), Sand flux in the northern Chihuahuan desert, New Mexico, USA, and the influence of mesquite-dominated landscapes, *J. Geophys. Res.*, *109*, F04003, doi:10.1029/2003JF000031.

Gillies, J. A., W. G. Nickling, and J. King (2002), Drag coefficient and plant form-response to wind speed in three plant species: Burning Bush (*Euonymus alatus*), Colorado Blue Spruce (*Picea pungens glauca.*), and Fountain Grass (*Pennisetum setaceum*), *J. Geophys. Res.*, *107*(D24), 4760, doi:10.1029/2001JD001259.

Gillies, J. A., W. G. Nickling, and J. King (2006), Aeolian sediment transport through large patches of roughness in the atmospheric inertial sublayer, *J. Geophys. Res.*, *111*, F02006, doi:10.1029/2005JF000434.

Gillies, J. A., W. G. Nickling, and J. King (2007), Shear stress partitioning in large patches of roughness in the atmospheric inertial sublayer, *Boundary Layer Meteorol.*, *122*(2), 10,367–10,396, doi:10.1007/s10546-10006-19101-10545.

Glendening, J. W. (1977), Aeolian transport and vegetative capture of particles, M.Sc. thesis, 121 pp, Colo. State Univ., Fort Collins.

Hinze, J. O. (1975), *Turbulence*, 790 pp., McGraw-Hill, New York.

Jackson, P. S. (1981), On the displacement height in the logarithmic profile, *J. Fluid Mech.*, *111*, 15–25.

Kaimal, J. C., and J. J. Finnigan (1994), *Atmospheric Boundary Layer Flows: Their Structure and Measurement*, 289 pp., Oxford Univ. Press, New York.

King, J., W. G. Nickling, and J. A. Gillies (2005), Representation of vegetation and other non-erodible elements in aeolian shear stress partitioning models for predicting transport threshold, *J. Geophys. Res.*, *110*, F04015, doi:10.1029/2004JF000281.

King, J., W. G. Nickling, and J. A. Gillies (2006), Aeolian shear stress ratio measurements within mesquite-dominated landscapes of the Chihuahuan Desert, New Mexico, USA, *Geomorphology*, *82*(3–4), 229–244.

Lettau, H. (1969), Note on aerodynamic roughness-parameter estimation on the basis of roughness-element description, *J. Appl. Meteorol.*, *8*, 828–832.

Macdonald, R. W., R. F. Griffiths, and D. J. Hall (1998), An improved method for the estimation of surface roughness of obstacle arrays, *Atmos. Environ.*, *32*(11), 1857–1864.

Marshall, J. K. (1971), Drag measurements in roughness arrays of varying densities and distribution, *Agric. Meteorol.*, *8*, 269–292.

Musick, H. B., S. M. Trujillo, and C. R. Truman (1996), Wind-tunnel modelling of the influence of vegetation structure on saltation threshold, *Earth Surf. Processes Landforms*, *21*(7), 589–605.

Raupach, M. R. (1994), Simplified expressions for vegetation roughness length and zero-plane displacement as functions of canopy height and area index, *Boundary Layer Meteorol.*, *71*, 211–216.

Raupach, M. R., R. A. Antonia, and S. Rajagopalan (1991), Rough-wall turbulent boundary layers, *Appl. Mech. Rev.*, *44*(1), 1–25.

Raupach, M. R., D. A. Gillette, and J. F. Leys (1993), The effect of roughness elements on wind erosion threshold, *J. Geophys. Res.*, *98*(D2), 3023–3029.

Raupach, M. R., D. E. Hughes, and H. A. Cleugh (2006), Momentum absorption in rough-wall boundary layers with sparse roughness elements in random and clustered distributions, *Boundary Layer Meteorol.*, *120*, 201–218.

Stull, R. B. (1988), *An Introduction to Boundary Layer Meteorology*, 665 pp., Kluwer Acad., Dordrecht, Netherlands.

Tennekes, H., and J. L. Lumley (1972), *A First Course in Turbulence*, 300 pp., MIT Press, Cambridge, Mass.

Thom, A. S. (1971), Momentum absorption by vegetation, *Q. J. R. Meteorol. Soc.*, *97*, 414–428.

Wilkinson, R. H. (1984), A method for evaluating statistical errors associated with logarithmic velocity profiles, *Geo Mar. Lett.*, *3*(1), 49–52.

J. A. Gillies, Particle Emissions Measurement Laboratory, Division of Atmospheric Sciences, Desert Research Institute, 2215 Raggio Parkway, Reno, NV 89512, USA. (jackg@dri.edu)

J. King, Division of Atmospheric Sciences, Desert Research Institute, 755 E. Flamingo Road, Las Vegas, NV 89119, USA. (james.king@dri.edu)

W. G. Nickling, Wind Erosion Laboratory, Department of Geography, University of Guelph, Guelph, ON, Canada N1G 2W1. (nickling@uoguelph.ca)